Catal Lett (2008) 123:294–300
DOI 10.1007/s10562-008-9422-8

Single-Crystalline $La_{0.6}Sr_{0.4}CoO_{3-\delta}$ Nanowires/Nanorods Derived Hydrothermally Without the Use of a Template: Catalysts Highly Active for Toluene Complete Oxidation

Jiguang Deng · Lei Zhang · Hongxing Dai · Hong He · Chak Tong Au

Received: 28 November 2007 / Accepted: 29 January 2008 / Published online: 12 February 2008

Abstract Single-crystalline nanowires and nanorods of cubic perovskite-type $La_{0.6}Sr_{0.4}CoO_{3-\delta}$ oxides have been fabricated by a hydrothermal method and characterized by a number of analytical techniques. Compared to the polycrystalline $La_{0.6}Sr_{0.4}CoO_{3-\delta}$ catalyst, the single-crystalline materials exhibit much better catalytic activity for the complete oxidation of toluene. The excellent performance can be attributed to the distinct oxygen nonstoichiometry and single-crystalline structure of the materials.

Keywords Single-crystalline perovskite-type oxide · Nanowires/nanorods · Toluene oxidation · Hydrothermal synthesis

1 Introduction

One-dimensional (1D) nanomaterials exhibit unusual properties such as peculiar morphology, restricted size, and large surface area [1]. Up to now, composite oxide nanowires and/or nanorods of $LaMO_3$ (M = Mn, Fe, Ni, Co) [2–4], $La_{1-x}Ca_xMnO_3$ [5, 6], and $CoFe_2O_4$ [7] have been synthesized by sol–gel method of hard-templating, and the size and shape of the products are usually determined by the adopted template. As an important strategy to fabricate 1D nanomaterials, the hydrothermal route has attracted much attention owning to its simplicity, cost-effectiveness, and high product yield. By means of a number of hydrothermal pathways, one can synthesize $La_{1-x}Sr_xMnO_3$ [8, 9], $BaTi_{1-x}Mn_xO_3$ [10], and $NiFe_2O_4$ [11] nanowires/nanorods. To the best of our knowledge, there is no report on the synthesis of perovskite-type oxide (ABO_3) $La_{0.6}Sr_{0.4}CoO_3$ nanowires or nanorods in the literature.

It is well known that ABO_3 materials have found applications in catalysis, solid-state fuel cell, and sensor due to their defective structures and excellent oxygen mobility. Among the materials, $La_{0.6}Sr_{0.4}CoO_{3-\delta}$ is one of the best-performing catalysts for the oxidation of carbon monoxide and hydrocarbons [12–15]. Most authors believe that the catalytic activity of such a kind of materials is related to factors such as structural defects, *B*-site ion redox ability, and specific surface area [12–16]. Unfortunately, most of the methods for the preparation of ABO_3 materials could only give rise to condense materials of low surface area, mainly due to the need of high-temperature calcination for the formation of the ABO_3 phase. In this article, we report a facile route capable of generating single-crystalline nanowires/nanorods of $La_{0.6}Sr_{0.4}CoO_{3-\delta}$. As a demonstration of catalytic activity, the materials were tested for the complete oxidation of toluene.

2 Experimental

2.1 Catalyst Preparation

In a typical synthesis of $La_{0.6}Sr_{0.4}CoO_{3-\delta}$ nanowires/nanorods, stoichiometric amounts of nitrates of lanthanum, strontium, and cobalt were dissolved in deionized (DI)

J. Deng · L. Zhang · H. Dai (✉) · H. He
Laboratory of Catalysis Chemistry and Nanoscience, Department of Chemistry and Chemical Engineering, College of Environmental and Energy Engineering, Beijing University of Technology, Beijing 100022, P.R. China
e-mail: hxdai@bjut.edu.cn

C. T. Au (✉)
Department of Chemistry, Hong Kong Baptist University, Kowloon Tong, Hong Kong, P.R. China
e-mail: pctau@hkbu.edu.hk

water, and 0.35 mol KOH solid powders were then added. After 1 h of ultrasonic stirring, the solution was transferred to a 50-mL Teflon-lined autoclave for hydrothermal treatment at 250 °C for 50 h. The so-obtained solid product was washed with DI water and dried overnight in an oven at 120 °C. The dried powders were well ground and heated in air at a rate of 1 °C/min in a muffle furnace to 400 °C and kept at this temperature for 2 h, and then heated to a selected temperature (650, 800, and 900 °C) and maintained at this temperature for 2 h. The as-obtained catalysts are denoted as LSCO-650, LSCO-800, and LSCO-900 hereinafter, respectively. For comparison purpose, we also prepared a polycrystalline $La_{0.6}Sr_{0.4}CoO_{3-\delta}$ catalyst adopting the citric acid-complexing procedure similar to that described in [15]. The polycrystalline $La_{0.6}Sr_{0.4}CoO_{3-\delta}$ sample (denoted as LSCO-950-Citrate) was calcined at 950 °C for 4 h. All the chemicals (analytical grade) were purchased from the Beijing Chemical Regent Company and were used without further purification.

2.2 Catalyst Characterization

X-ray diffraction (XRD) patterns of the catalysts were recorded on a Bruker/AXS D8 Advance X-ray diffractometer operated at 40 kV and 200 mA using Cu$K\alpha$ radiation and Ni filter. Diffraction peaks of crystal phases were referred to those of 1998 ICDD PDF Database for identification. The surface areas of the catalysts were measured via N_2 adsorption at −196 °C on an ASAP 2020 apparatus. X-ray photoelectron spectroscopy (XPS, VG CLAM 4 MCD analyzer, Mg$K\alpha$ = 1253.6 eV) was used to determine the O1s, Co2p, La3d, and Sr3d binding energy (BE) of surface oxygen, cobalt, lanthanum, and strontium species, respectively. The C1s signal at 284.6 eV was taken as a reference for BE calibration. High-resolution scanning electron microscopy (HRSEM) images of the samples were recorded using a JEOL JSM 6500F equipment operated at a 30 kV accelerating voltage. By means of a JEOL-2010 instrument (operating at 200 kV), high-resolution transmission electron microscopy (HRTEM) images and selected area electron diffraction (SAED) patterns of the samples were obtained.

Oxygen temperature-programmed desorption (O_2-TPD) profiles of the samples were recorded on a mass spectrometer (HIDEN HPR20). For O_2-TPD studies, the sample (0.1–0.2 g) was placed in the middle of a quartz microreactor (internal diameter (i.d.) = 8 mm). The outlet gases were analyzed on-line by means of a mass spectrometer. The heating rate was 10 °C/min and the temperature range was RT to 900 °C. Before each run, the sample was calcined at 500 °C in an O_2 flow of 50 mL/min for 1 h, followed by cooling in oxygen to RT and purging with helium (first 80 mL/min for 2 h and then 20 mL/min for 2 h). The helium-purging step is to ensure thorough removal of gas-phase oxygen in the system. The amount of O_2 desorbed from the catalyst was quantified by calibrating the peak area against that of a standard O_2 pulse (50.0 μL).

2.3 Catalytic Test

The catalytic evaluation was conducted on a continuous flow fixed-bed quartz microreactor (i.d. = 8 mm) at atmospheric pressure. The catalyst (0.1 g, 40–60 mesh) was mixed properly with equal amount (by mass) of quartz sands (40–60 mesh), and the reactant mixture (flow rate = 33.3 mL/min) was 1,000 ppm toluene + O_2 + N_2 (balance), bearing a toluene/O_2 molar ratio of 1/400 and a space velocity of 20,000 h^{-1}. For the change of space velocity, we altered the amount of catalyst. The outlet gases were analyzed on-line by a gas chromatograph (Shimadzu GC-2010) equipped with a thermal conductivity detector, using a Chromosorb 101 column for toluene and a Carboxen 1000 column for permanent gas separation. The balance of carbon throughout the investigation was estimated to be 99.5%.

3 Results and Discussion

3.1 Characterization

3.1.1 Crystal Structures, Surface Areas, and Morphologies of Catalysts

The XRD patterns (Fig. 1) of the samples show peaks with positions and relative intensities consistent with those of cubic $LaCoO_3$ (JCPDS No.: 75-0279), and the diffraction peaks can be well-indexed as indicated in Fig. 1c. The rather weak peak at 2θ = ca. 25.3° is attributable to the phase of La_2O_3 (JCPDS No.: 83-1355) that existed as impurity. The intensity of the 25.3° peak decreased with the rise in calcination temperature. Apparently, the as-obtained samples contained predominantly cubic perovskite-type $La_{0.6}Sr_{0.4}CoO_{3-\delta}$. It is known that La_2O_3 is inactive for the oxidation of organic compounds. Nevertheless, its presence would undermine the activation of oxygen molecules, and cause a slight decrease in catalytic activity of the ABO_3 material.

Representative HRSEM and HRTEM images as well as SAED patterns are shown in Fig. 2. It is observed that the LSCO-650 sample consists of a large amount of uniform $La_{0.6}Sr_{0.4}CoO_{3-\delta}$ nanowires (typical diameter = 15–30 nm) (Fig. 2a). A mixture of nanorods and nanowires (Fig. 2c and d) is obtained after calcination at 800 °C, and the typical diameters of nanorods and nanowires fall into

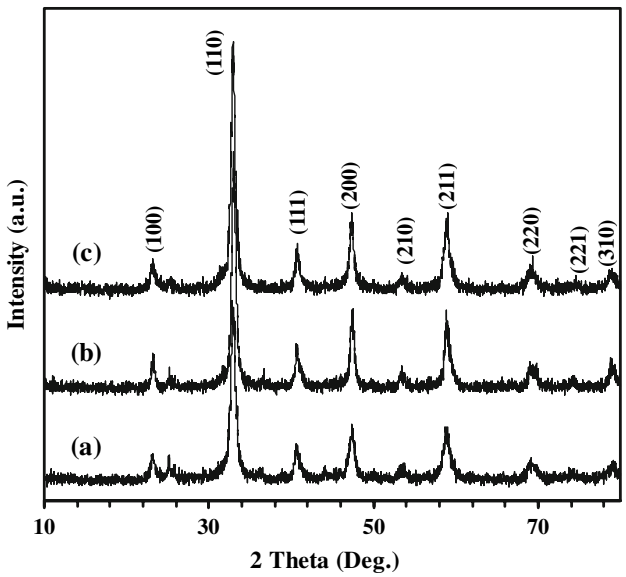

Fig. 1 XRD patterns of (**a**) LSCO-650, (**b**) LSCO-800, and (**c**) LSCO-900

the range of 15–35 and 20–85 nm, respectively. Further rise in calcination temperature to 900 °C would result in a rod-like morphology, and the typical aspect ratio equals to ca. 6. Obviously, calcination temperature has a significant influence on the morphology of the $La_{0.6}Sr_{0.4}CoO_{3-\delta}$ materials. The corresponding SAED patterns (insets of Fig. 2b, d, f) show regularly aligned lines of bright spots, disclosing that the $La_{0.6}Sr_{0.4}CoO_{3-\delta}$ nanowires and nanorods are well-grown single crystallites. According to the HRTEM photographs (Fig. 2g, h, i), the *d* spacings of the (110) and (200) planes are estimated to be 0.275 and 0.194 nm, respectively, not far away from the corresponding values (0.271, 0.192 nm) of cubic perovskite-type cobaltite polycrystallites (JCPDS No.: 75-0279).

The surface area of the LSCO-650, LSCO-800, LSCO-900, and LSCO-950-Citrate sample is 30.7, 15.4, 8.2, and 4.2 m^2/g, respectively. As expected, the size growth of the particles and the morphological evolution of the samples (from nanowires to nanorods) at elevated calcination temperatures (Fig. 2) result in significant drop in specific surface area. Nevertheless, it is noted that the surface area of $La_{0.6}Sr_{0.4}CoO_{3-\delta}$ nanowires obtained after calcination at 650 °C is much bigger than that of the 650 °C-calcined $La_{0.6}Sr_{0.4}CoO_{3-\delta}$ nanoparticles obtained by citric acid complexing method (17.1 m^2/g) or by the citric acid complexing-hydrothermal synthesis coupled method (20.2 m^2/g) reported by Niu et al. [15].

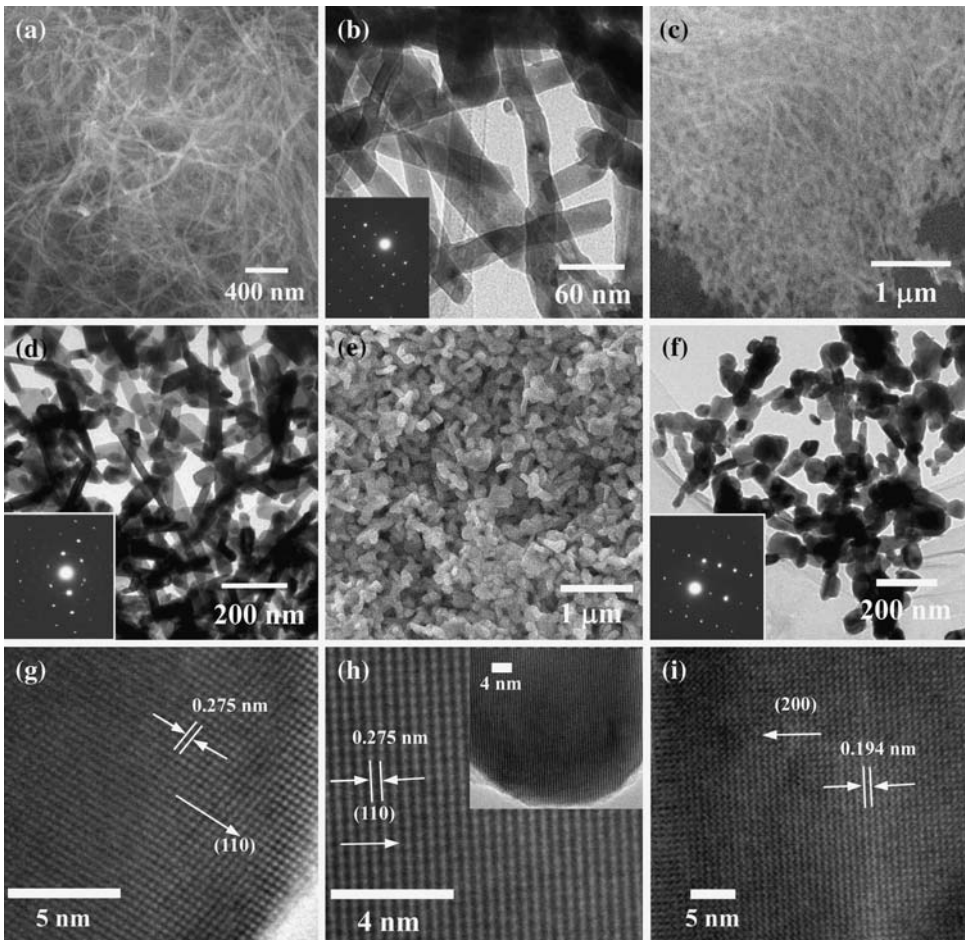

Fig. 2 HRSEM (**a**, **c**, **e**), HRTEM (**b**, **d**, **f**-**i**) images and SAED patterns (*insets*) of LSCO-650 (**a**, **b**), LSCO-800 (**c**, **d**), and LSCO-900 (**e**-**i**)

According to the results and discussion of Hu et al. [10], Chu et al. [11], and Cao et al. [17], we deduced that the possible reaction mechanism for the hydrothermal synthesis of $La_{0.6}Sr_{0.4}CoO_{3-\delta}$ is as follows:

$$La(NO_3)_3 + 3KOH \rightarrow La(OH)_3 + 3K(NO_3) \quad (1)$$

$$Sr(NO_3)_2 + 2KOH \rightarrow Sr(OH)_2 + 2K(NO_3) \quad (2)$$

$$Co(NO_3)_2 + 2KOH \rightarrow Co(OH)_2 + 2K(NO_3) \quad (3)$$

$$0.6La(OH)_3 + 0.4Sr(OH)_2 + Co(OH)_2 \rightarrow La_{0.6}Sr_{0.4}CoO_{3-\delta} + 2.3H_2O \quad (4)$$

During hydrothermal treatment in a strongly basic medium, there is the growth of the $La_{0.6}Sr_{0.4}CoO_{3-\delta}$ nanostructure, and the formation of three-dimensional $La_{0.6}Sr_{0.4}CoO_{3-\delta}$ particles is suppressed. This is likely to be the key factor for the generation of $La_{0.6}Sr_{0.4}CoO_{3-\delta}$ nanowires. Similar mechanism has also been proposed for the growth of nanowires of various metal oxides [10, 18, 19].

3.1.2 XPS

Shown in Fig. 3 are the O1s and $Co2p_{3/2}$ XPS spectra of the samples. There are three O1s signals at BE = 529.6–529.9, 531.4–531.9, and 533.1–533.6 eV. The one at BE = 529.6–529.9 eV was attributed to surface lattice oxygen ($O^{2-}_{lattice}$) [15, 20, 21] and the one at BE = 533.1–533.6 eV to adsorbed molecular water species [22]. In the preparation of single-crystalline catalysts, no carbon-containing precursors were used. We detected no C1s signal at BE = ca. 289 eV over the single-crystalline catalysts whereas over LSCO-950-Citrate, C1s signal at ca. 289 eV of carbonate was detected (not shown). We hence deduced that the O1s signal at BE = ca. 531.4–531.9 eV detected over the single-crystalline catalysts is not due to CO_3^{2-} species. It is difficult to differentiate adsorbed oxygen (O^-, O^{2-} or O_2^{2-}) from OH^- species based solely on BE values. Nevertheless, most authors believed that the oxygen adspecies on perovskite-type oxides are located at oxygen vacancies mainly in the form of O^-, O^{2-} or O_2^{2-}. We hence ascribe the O1s component of our single-crystalline catalysts at BE = ca. 531.4–531.9 eV to adsorbed oxygen species (O^-, O^{2-}, O_2^{2-} or OH^-) [15, 20, 21]. Based on the results of Fig. 3A, we found that the surface $O_{ads}/O^{2-}_{lattice}$ ratios of LSCO-650, LSCO-800, LSCO-900, and LSCO-950-Citrate are 1.6, 1.8, 2.2, and 1.2, respectively. It is apparent that higher in calcination temperature would result in larger portion of oxygen adspecies, and the single-crystalline catalysts are more capable of activating O_2 than the polycrystalline one. It is known that oxygen adspecies dwell preferentially at oxygen vacancies of ABO_3 materials. Hence, an increase in amount of oxygen adspecies would suggest enhancement in density of oxygen vacancies. We deduce that with rise of calcination temperature, there is promoted generation of oxygen vacancies. The enlarged presence of oxygen vacancies favors the adsorption and activation of O_2.

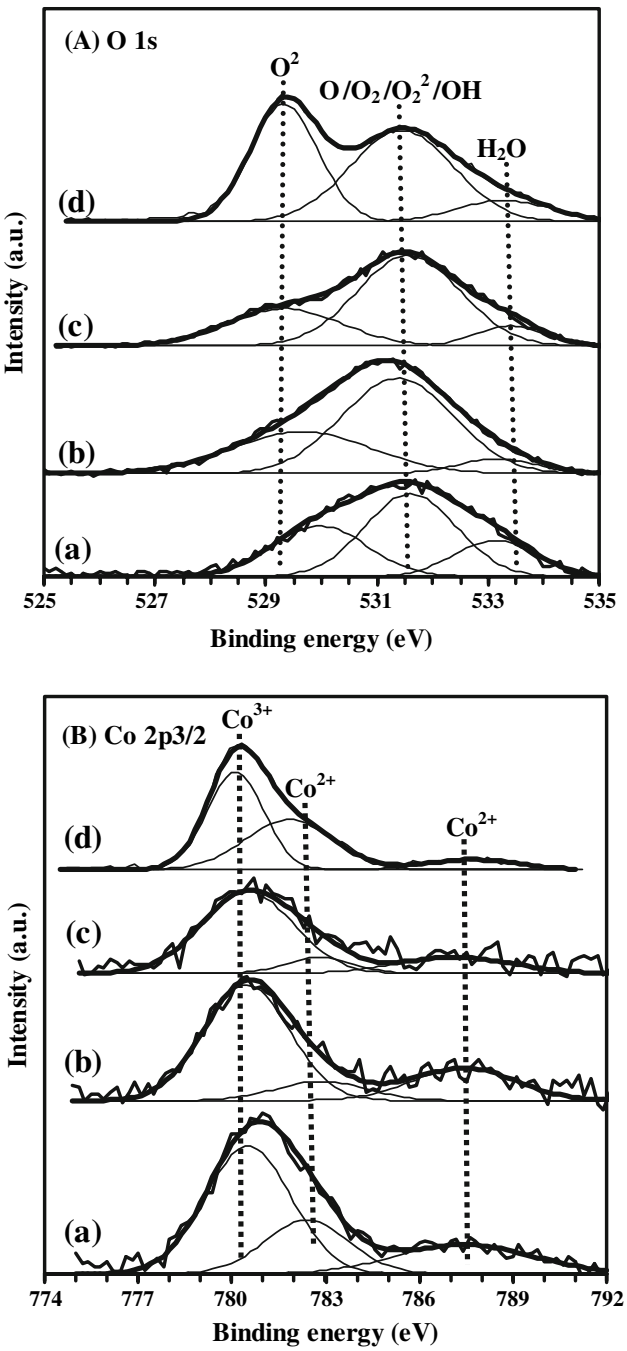

Fig. 3 (**A**) O1s and (**B**) $Co2p_{3/2}$ XPS spectra of (**a**) LSCO-650, (**b**) LSCO-800, (**c**) LSCO-900, and (**d**) LSCO-950-Citrate

In XPS investigation over oxidic compounds containing Co^{2+} and Co^{3+} ions, Fierro et al. observed an inverse shift of main peak positions of Co^{2+} and Co^{3+} [23]. After deconvolution of the Co $2p_{3/2}$ profile of cobalt–zinc hydroxycarbonates, Baird et al. [24] assigned the signal at

BE = 780.1 and 782.1 eV to Co^{3+} and Co^{2+}, respectively. Working over $La_{0.8}Sr_{0.2}CoO_3$, Gunasekaran et al. suggested that the signal at BE = 779.4 eV was due to Co^{3+} [25]. We found that the separation of $Co2p_{3/2}$ and $Co2p_{1/2}$ peaks due to spin-orbit splitting over $La_{0.6}Sr_{0.4}CoO_{3-\delta}$ (not shown here) was 15.2 eV, coinciding with that observed over $La_{0.8}Sr_{0.2}CoO_3$ by Gunasekaran et al. From Fig. 3B, one can observe signals at BE = ca. 780.5 and 782.5 eV with a satellite peak at ca. 787.5 eV (characteristic of Co^{2+}). According to the aforementioned viewpoints [23–26], we believe that it is reasonable to ascribe the signal at BE = 780.5 eV to Co^{3+} and that at BE = 782.5 eV to Co^{2+}. One can also observe that with a rise in calcination temperature, the intensity of Co^{2+} satellite signal decreased, indicating a drop of Co^{2+} concentration. The surface Co^{3+}/Co^{2+} ratio was estimated to be 1.3, 2.0, and 2.5 for LSCO-650, LSCO-800, and LSCO-900, respectively. It is apparent that a rise in calcination temperature promotes the generation of cobalt ions of trivalency.

3.1.3 O_2-TPD

The O_2-TPD profiles of $La_{0.6}Sr_{0.4}CoO_{3-\delta}$ samples are shown in Fig. 4. There is a weak broad desorption peak at 390 °C and a sharp peak at 875 °C over the LSCO-650 sample. Over the LSCO-800 sample, there are three peaks at 225, 515, and 794 °C. In the case of LSCO-900, two peaks were recorded, one at 340 °C and the other at 831 °C. As for the LSCO-950-Citrate sample, three peaks at 280, 540, and 830 °C were observed. The total amount of oxygen desorption below 650 °C (inset of Fig. 4) is estimated to be 31.2, 46.0, 69.3, and 13.2 μmol/g_{cat} for the LSCO-650, LSCO-800, LSCO-900, and LSCO-950-Citrate samples, respectively. According to Seiyama [13], the broad desorption peaks below 650 °C can be ascribed to α desorption originated from oxygen species adsorbed at oxygen vacancies. Thus, the extent of α desorption can be used to provide a rough estimation of the amount of oxygen vacancies on the surface of each sample. Accordingly, we deduced that the surface oxygen vacancy density of the three samples decreases in the order of LSCO-900 > LSCO-800 > LSCO-650 > LSCO-950-Citrate, in concord with the sequence of catalytic performance as shown in the next section.

3.2 Catalytic Performance

In the low-temperature oxidation of hydrocarbons, oxygen adspecies have an important role to play [12, 13]. Figure 5 shows the catalytic activities of the three $La_{0.6}Sr_{0.4}CoO_{3-\delta}$ samples for the oxidation of toluene under the conditions of toluene concentration = 1,000 ppm, toluene/O_2 molar ratio = 1/400, and space velocity = 20,000 h^{-1}. The toluene conversion increases with increasing reaction temperature, and the LSCO-900 catalyst performs the best. The light-off temperature $T_{50\%}$ (conversion = 50%) and

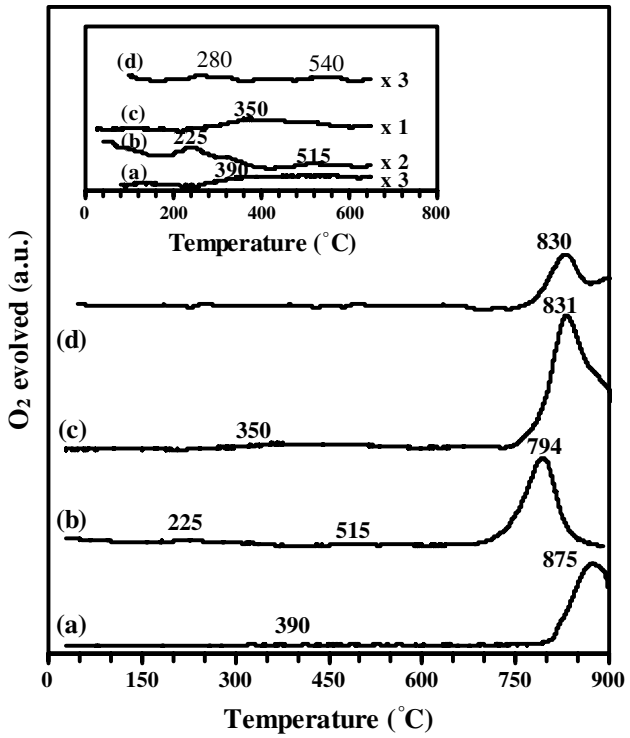

Fig. 4 O_2-TPD profiles of (**a**) LSCO-650, (**b**) LSCO-800, (**c**) LSCO-900, and (**d**) LSCO-950-citrate. Inset is the enlarged profiles below 650 °C

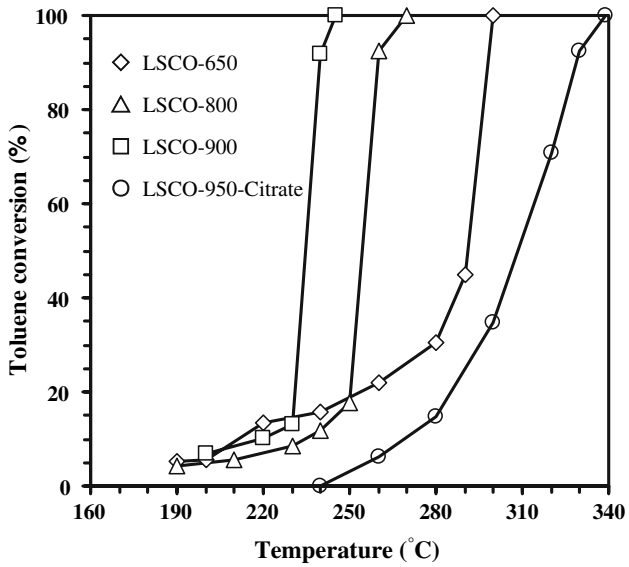

Fig. 5 Catalytic performance (at a space velocity of 20,000 h^{-1}) versus reaction temperature over LSCO-650, LSCO-800, LSCO-900, and LSCO-950-citrate

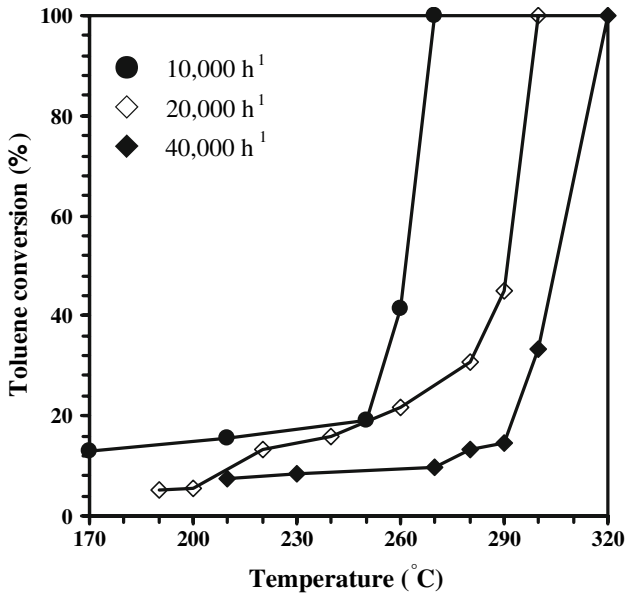

Fig. 6 Catalytic performance versus reaction temperature over LSCO-650 at different space velocities

the temperature for complete toluene removal $T_{100\%}$ (conversion = 100%) are, respectively, 235 and 245 °C over LSCO-900, 255, and 270 °C over LSCO-800, and 292 and 300 °C over LSCO-650. Obviously, the enhancement in catalytic activity of the samples can be related to the rise in calcination temperature. The variation of surface area seems to have no direct effect on the catalytic performance. That is to say, the catalysis of the target reaction is determined by the oxygen deficiency of the materials. The single-crystalline $La_{0.6}Sr_{0.4}CoO_{3-\delta}$ materials show catalytic activities much better than the polycrystalline $LaMnO_3$ and $La_{0.8}Sr_{0.2}MnO_3$ samples ($T_{100\%} > 340$ °C even at a rather low space velocity of 184 h^{-1}) [14]. From Fig. 5, one can also observe that the $T_{50\%}$ and $T_{100\%}$ value over LSCO-950-Citrate was 306 and 339 °C, respectively. Clearly, the polycrystalline catalyst is much inferior to its single-crystalline counterparts. The discrepancy in activity can be related to the difference in oxygen nonstoichiometry. As expected, with an increase in space velocity (i.e., shortening contact time), the $T_{50\%}$ and $T_{100\%}$ value over the LSCO-650 sample increase (Fig. 6). It is worth pointing out that the products detected over the single-crystalline ABO_3 nanowires and nanorods in the oxidation of toluene are entirely CO_2 and H_2O, as confirmed by an estimated carbon balance of 99.5%.

4 Conclusion

In summary, single-crystalline $La_{0.6}Sr_{0.4}CoO_{3-\delta}$ nanowires and nanorods with a cubic perovskite structure have been fabricated by a simple hydrothermal method. The calcination temperature has a significant influence on the morphology of the $La_{0.6}Sr_{0.4}CoO_{3-\delta}$ materials. The surface area of $La_{0.6}Sr_{0.4}CoO_{3-\delta}$ nanowires is much higher than that of $La_{0.6}Sr_{0.4}CoO_{3-\delta}$ nanorods. The single-crystalline perovskites exhibit excellent catalytic performance for the complete oxidation of toluene, with the $La_{0.6}Sr_{0.4}CoO_{3-\delta}$ nanorods performing the best. We deduced that the excellent performance is attributable to the oxygen vacancy density and the unique single-crystalline structures rather than to the specific surface area. The synthesis strategy presented here can be adopted as an effective means for the generation of ABO_3 of similar kind.

Acknowledgments The work was supported by the Natural Science Foundation of Beijing Municipality (Key Class B project of grant number KZ200610005004). CTA thanks the RGC, Hong Kong Special Administration Region for financial support (Grant HKBU 200106).

References

1. Alivisatos AP (1996) Science 271:933
2. Yang Z, Huang Y, Dong B, Li HL (2005) Appl Phys A 81:453
3. Yang Z, Huang Y, Dong B, Li HL, Shi SQ (2006) Appl Phys A 84:117
4. Hu ZA, Wu HY, Shang XL, Lu RQ, Li HL (2006) Mater Res Bull 41:1045
5. Ma XY, Zhang H, Xu J, Niu JJ, Yang Q, Sha J, Yang DR (2002) Chem Phys Lett 363:579
6. Shankar KS, Kar S, Raychaudhuri AK, Subbanna GN (2004) Appl Phys Lett 84:993
7. Ji GB, Tang SL, Xu BL, Gu BX, Du YW (2003) Chem Phys Lett 379:484
8. Zhu D, Zhu H, Zhang YH (2002) J Phys Condens Matter 14:L519
9. Liu JB, Wang H, Zhu MK, Wang B, Yan H (2003) Mater Res Bull 38:817
10. Hu CG, Liu H, Lao CS, Zhang LY, Davidovic D, Wang ZL (2006) J Phys Chem B 110:14050
11. Chu XF, Jiang DL, Zheng CM (2007) Sens Actuat B 123:793
12. Seiyama T (1992) Catal Rev Sci Eng 34:281
13. Seiyama T (1993) In: Tejuca LG, Fierro JLG (eds) Properties and applications of Perovskite-type oxides, ch. 10. Dekker, New York
14. Irusta S, Pina MP, Menéndez M, Santamaría J (1998) J Catal 179:400
15. Niu JR, Liu W, Dai HX, He H, Zi XH, Li PH (2006) Chin Sci Bull 51:1673
16. Barnard KR, Foger K, Turney TW, Williams RD (1990) J Catal 125:265
17. Cao MH, Hu CW, Peng G, Qi YJ, Wang EB (2003) J Am Chem Soc 125:4982
18. Urban JJ, Ouyang L, Jo M, Wang DS, Park H (2004) Nano Lett 4:1547
19. Wang X, Li Y (2002) Angew Chem Int Ed 41:4790
20. Carley AF, Roberts MW, Santra AK (1997) J Phys Chem B 101:9978
21. Yamazoe N, Teraoka Y, Seiyama T (1981) Chem Lett 1767
22. Fierro JLG, Tejuca LG (1987) Appl Surf Sci 27:453

23. Fierro G, Lo Jacono M, Inversi M, Dragone R, Porta P (2000) Top Catal 10:39
24. Baird T, Campbell KC, Holliman PJ, Hoyle RW, Stirling D, Williams BP, Morris M (1997) J Mater Chem 7:319
25. Gunasekaran N, Bakshi N, Alcock CB, Carberry JJ (1996) Solid State Ionics 83:145
26. O'Connell M, Norman AK, Hüttermann CF, Morris MA (1999) Catal Today 47:123